Perfect Lensing by a Single Interface: Defying Loss and Bandwidth Limitations of Metamaterials

Gilad Rosenblatt and Meir Orenstein*
Department of Electrical Engineering, Technion, Haifa 32000, Israel
(Received 25 May 2015; published 5 November 2015)

Loss is known to be detrimental for achieving perfect focusing with the passive perfect lens designs suggested thus far, and it is believed to pose a fundamental barrier. We show that perfect lensing can be achieved with actual lossy left-handed metamaterials, without a need for gain or nonlinearity. The proposed loss-immune perfect lens is composed of a single interface between a conventional dielectric material on the source side and a lossy left-handed material on the image side. Its immunity to material loss was derived analytically using three complementary methodologies, confirming perfect lensing with point-to-point accuracy and shedding light on the underlying focusing mechanism. This result provides a new road map for practical realization of a near-field camera based on the single-interface lens design.

DOI: 10.1103/PhysRevLett.115.195504 PACS numbers: 81.05.Xj, 73.20.Mf, 78.67.Pt

Introduction.—The diffraction of light in conventional media limits light focusing to spots roughly half-wavelength in diameter [1]. This barrier is associated with the inability to collect the near-field evanescent spatial spectrum. The advent of composite electromagnetic media possessing negative values of both effective permittivity and permeability challenged this paradigm [2–5]. In such media the electric field, magnetic fields, and wave vector of plane waves form a left-handed set. This results in a Poynting vector antiparallel to the wave vector, and in negative refraction at interfaces with regular materials. Hence, a slab made of a left-handed metamaterial acts as a flat lens [2]. Furthermore, if perfectly impedance matched, it performs, in principle, as a perfect lens [6]. Such a lens would be capable of collecting the entire spatial frequency range (including the evanescent), thereby having no inherent limit to its focusing capability.

The perfect lens idea stimulated a great deal of research aimed at its realization [7–9]. However, a fundamental obstacle lies in the fact that left-handed materials are intrinsically highly dispersive and therefore lossy, whereas the perfect lens relies on the availability of lossless (noncausal) left-handed materials. This is because its subdiffraction focusing capability degrades exponentially with any deviation from matching, incurred by even small loss [10–17].

Presently, therefore, perfect lensing is being pursued by alternative approaches. One approach aims to mimic the boundary conditions imposed by a left-handed slab using a pair of phase-conjugating interfaces which requires sufficiently strong nonlinearity [18–21], for example, by using four-wave mixing in graphene sheets to produce negative refraction [22,23]. Another approach employs a pair of parity-time-symmetric metasurfaces instead, avoiding nonlinearity but introducing optical gain [24,25]. Maxwell's fish-eye lens, constructed entirely of a positively refracting inhomogeneous medium, can also act as a perfect lens [26,27].

Here we show that perfect lensing can be achieved using a passive, lossy, left-handed metamaterial by applying a single-interface configuration. The proposed lens is composed of only one interface, between a dielectric and a realizable (lossy, causal) left-handed metamaterial. It proves surprisingly resilient with a perfect focal plane, and does not require the use of nonlinear effects or gain media.

We arrive at this result by examining the single-interface lens using three types of complementary closed-form methodologies: transmission analysis to derive its basic diffraction characteristics (see section "Single interface as a spatial all-pass filter"), Green's function analysis to study its actual lensing capability (see section "Loss-immune point-to-point imaging"), and modal analysis for further insight into its lensing mechanism (see section "Modal interpretation for perfect lensing"). They all consistently show that the single-interface lens generates a singular focal spot, even with material loss, making it a loss-immune perfect lens.

Single interface as a spatial all-pass filter.—Consider an incoming TE-polarized plane wave of angular frequency ω and spatial frequency β (z wave vector component) impinging on a single interface between a dielectric (double positive, DPS) and a left-handed medium (double negative, DNG) at $x = 0$ [Fig. 1(a)]. The y-directed electric field phasor $\mathbf{E} = f(x)e^{-j\beta z}\mathbf{y}$ can be written as a sum of incident (from the DPS side) reflected and transmitted waves ($e^{j\omega t}$ convention),

$$f(x) = \begin{cases} e^{-jk_{x,\mathrm{DPS}}x} + re^{jk_{x,\mathrm{DPS}}x} & x < 0 \\ te^{-jk_{x,\mathrm{DNG}}x} & x > 0, \end{cases} \quad (1)$$

where $k^2_{x,\mathrm{DNG,DPS}} = (\omega/c)^2\varepsilon_{\mathrm{DNG,DPS}}\mu_{\mathrm{DNG,DPS}} - \beta^2$ is the x wave vector component in the DNG and DPS media,

respectively, $\varepsilon_{\mathrm{DNG,DPS}}$ and $\mu_{\mathrm{DNG,DPS}}$ are the relative media permittivities and permeabilities, c is the speed of light in vacuum, and the field amplitude reflection (r) and transmission (t) coefficients are given by

$$r = \frac{k_{x,\mathrm{DPS}}/\mu_{\mathrm{DPS}} - k_{x,\mathrm{DNG}}/\mu_{\mathrm{DNG}}}{k_{x,\mathrm{DPS}}/\mu_{\mathrm{DPS}} + k_{x,\mathrm{DNG}}/\mu_{\mathrm{DNG}}},$$
$$t = \frac{2k_{x,\mathrm{DPS}}/\mu_{\mathrm{DPS}}}{k_{x,\mathrm{DPS}}/\mu_{\mathrm{DPS}} + k_{x,\mathrm{DNG}}/\mu_{\mathrm{DNG}}}. \quad (2)$$

Generally, there are two branch choices to consider for each of $k_{x,\mathrm{DNG}}$ and $k_{x,\mathrm{DPS}}$. We take the root branches such that $\mathrm{Im}\{k_{x,\mathrm{DNG}}\} > 0$ and $\mathrm{Im}\{k_{x,\mathrm{DPS}}\} < 0$, a choice we thoroughly justify in the next section, when we consider the Green's function.

We first examine the matched case, defined as $\varepsilon_{\mathrm{DNG}} = -\varepsilon_{\mathrm{DPS}}$ and $\mu_{\mathrm{DNG}} = -\mu_{\mathrm{DPS}}$ (implying impedance matching $\mu_{\mathrm{DPS}}/\varepsilon_{\mathrm{DPS}} = \mu_{\mathrm{DNG}}/\varepsilon_{\mathrm{DNG}}$ and lossless materials). With the aforementioned branch choice, the transverse wave vector component undergoes a sign shift at the interface ($k_{x,\mathrm{DNG}} = -k_{x,\mathrm{DPS}}$), regardless of β. Hence, all wave vector components perpendicular to the interface—propagating and evanescent—invert. This leads to uniform reflectionless transmission across all spatial frequencies, as Eq. (2) becomes $r = 0$, $t = 1$ for all β.

For the matched case, the slab and single-interface lenses act similarly: they perform as uniform spatial all-pass filters and are therefore expected to act as perfect lenses. The principle difference between the two lenses, however, lies in their respective performance under mismatched conditions. While the slab lens resolution severely degrades when material loss or frequency offsets from the matching frequency are introduced [10–17], the single-interface lens resolution does not. In fact, we show that it maintains perfect resolution under realistic deviations from the matching condition, whether these are due to material loss or frequency offsets—i.e., it is both loss immune and broadband.

From a plane wave (both uniform and nonuniform) point of view, such robustness requires that the field amplitude transmission coefficient maintains an asymptotically uniform unbounded form; i.e., it must not exhibit a spatial cutoff. Indeed, for large β values ($\beta \gg \omega/c$, $k_{x,\mathrm{DPS}} \approx -j|\beta|$, $k_{x,\mathrm{DNG}} \approx +j|\beta|$), the transmission is asymptotically uniform, approaching a finite value even when the matching condition does not exactly hold:

$$t_\infty = \lim_{\beta\to\infty} t = 2/(1 - \mu_{\mathrm{DPS}}/\mu_{\mathrm{DNG}}). \quad (3)$$

Figure 1 compares the single-interface and slab field-amplitude transmission functions [Figs. 1(a) and 1(b)], calculated using effective DNG parameters from two existing implementations: (1) a low-loss printed circuit board in the microwave regime [figure of merit: FOM $= |\mathrm{Re}\{n_{\mathrm{DNG}}\}/\mathrm{Im}\{n_{\mathrm{DNG}}\}| \approx 30$ at 2.4 GHz, Fig. 1(c)] [28], and (2) a higher-loss fishnet structure in the near IR

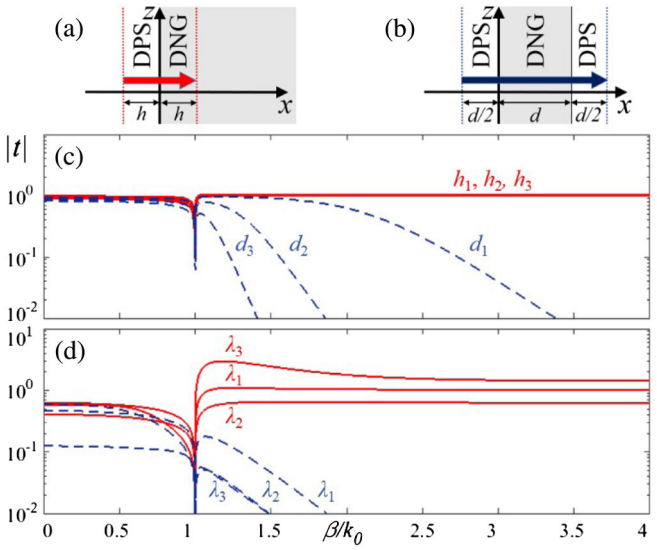

FIG. 1 (color online). TE amplitude transmission functions (logarithmic versus β) of an air-DNG single interface [illustration (a), red lines in (c) and (d)] and a DNG slab [illustration (b), dashed blue lines in (c) and (d)], for $d = 2h$, calculated based on effective DNG parameters reported in the literature for two implementations: (c) at microwave frequency $\omega = 2\pi \times 2.4$ GHz ($\varepsilon_{\mathrm{DNG}} = -1$–$0.02i$, $\mu_{\mathrm{DNG}} = -1$–$0.06i$) [28], for $d_{1,2,3} = \lambda/3, 2d_1, 3d_1$, and (d) at near-IR wavelengths $\lambda_1 = 1.4$ μm, $\lambda_{3,2} = \lambda_1 \pm 32$ nm ($\varepsilon_{\mathrm{DNG},1,2,3} = -1.38$–$0.08i$, -1.15–$0.08i$, -1.62–$0.01i$, $\mu_{\mathrm{DNG},1,2,3} = -0.79$–$0.52i$, -0.32–$0.21i$, -1.58–$2.36i$) [29], for $d = \lambda_1/3$. Mismatch is minimized at λ_1 ($\mathrm{Re}\{n_{\mathrm{DNG},1,2,3}\} \approx -1, -0.6, -1.9$).

[FOM ≈ 3 at 1.4 μm, Fig. 1(d)] [29]. Mismatch sensitivity renders the slab loss sensitive and narrow band, as its transmission degrades whenever loss is increased [Fig. 1(d) versus Fig. 1(c)], the frequency is offset [$\lambda_{2,3}$ versus λ_1 in Fig. 1(d)], or the slab is made thicker [$d_{1,2,3}$ in Fig. 1(c)]. Consequently, the slab shows a cutoff at $\sim 3k_0$ (at best) in the microwave, and no subdiffraction capabilities in the near IR. This sensitivity does not exist for the single-interface configuration, which maintains an asymptotically uniform transmission in all cases, consistent with Eq. (3). Though not exactly 1, its relative uniformity over the entire evanescent spatial frequency range is what counts towards perfect lensing—as we argue in detail in the next section.

Loss-immune point-to-point imaging.—We now examine the single-interface response to excitation by a source, and show that it is perfectly reconstructed at the image. Since any physical source can be superimposed from point dipoles (3D) or current lines (2D), it is sufficient to study the system response to such infinitely localized excitations, i.e., the Green's function. Perfect reproduction of these singular sources means that their singularity is reproduced at the image.

We consider the stationary case of a current line source $\mathbf{J} = I_0\delta(x + h)\delta(z)\mathbf{y}$, located a distance h from a lossless matched DPS-DNG interface ($x = 0$) in the DPS side

($x < 0$), and show that its logarithmic singularity is reproduced at the image. The transverse electric field component E_y satisfies the Helmholtz equation,

$$[\partial_x^2 + \partial_z^2 + \varepsilon(x)\mu(x)(\omega/c)^2]E_y(x,z) = 0, \quad (4)$$

everywhere except at the object and image planes ($x = \pm h$). We employ the z-coordinate Fourier space, where the nonzero component of the vector potential $\psi(x,z)$ [$E_y = -j\omega\psi(x,z)$] is retrieved by summing over the field contributions $g(x,\beta)$ of all spatial components β emitted by the source:

$$\psi(x,z) = \frac{1}{2\pi}\int_{-\infty}^{\infty} g(x,\beta)e^{-j\beta z}d\beta. \quad (5)$$

The source-side ($x < 0$) equation then becomes

$$(\partial_x^2 + k_{x,\mathrm{DPS}}^2)g(x,\beta) = -\mu_0\mu_{\mathrm{DPS}}I_0\delta(x+h), \quad (6a)$$

and in between the interface and image plane ($0 < x < h$)

$$(\partial_x^2 + k_{x,\mathrm{DNG}}^2)g(x,\beta) = 0, \quad (6b)$$

where $k_{x,\mathrm{DNG,DPS}}^2 = (\omega/c)^2\varepsilon_{\mathrm{DNG,DPS}}\mu_{\mathrm{DNG,DPS}} - \beta^2$, and μ_0 is the vacuum permeability.

Applying boundary conditions at the interface [continuity of $g(x,\beta), \partial_x g(x,\beta)/\mu(x)$] and accounting for the singularity at the source [a $-\mu_0\mu I_0$ jump in $\partial_x g(x,\beta)$], yields the formal solution at the source-side

$$g(x,\beta) \underset{x<0}{=} \frac{2\psi_0}{k_{x,\mathrm{DPS}}}(e^{-jk_{x,\mathrm{DPS}}|x+h|} + re^{+jk_{x,\mathrm{DPS}}(x-h)}), \quad (7a)$$

and in between the interface and the image plane

$$g(x,\beta) \underset{0<x<h}{=} \frac{2\psi_0}{k_{x,\mathrm{DPS}}}te^{-j(k_{x,\mathrm{DNG}}+k_{x,\mathrm{DPS}})h}e^{-jk_{x,\mathrm{DNG}}(x-h)}, \quad (7b)$$

where r,t are the transmission and reflection coefficients [Eq. (2)], and $\psi_0 = \mu_0\mu_{\mathrm{DPS}}I_0/4j$.

Before we can inspect the solution at the image plane and beyond it, we must resolve the ambiguity in Eq. (5), in both the path of integration and the root branches (Riemann sheets) for $k_{x,\mathrm{DNG}}$, $k_{x,\mathrm{DPS}}$ along which this integration is carried. To guarantee that power properly emanates outward from the source in the DPS medium, the branch choice for $k_{x,\mathrm{DPS}}$ is such that the field contribution by any (evanescent) spatial component decays away from the source ($\mathrm{Im}\{k_{x,\mathrm{DPS}}\} < 0$).

The branch choice for $k_{x,\mathrm{DPS}}$ is more subtle. In the matched case ($\varepsilon_{\mathrm{DNG}} = -\varepsilon_{\mathrm{DPS}}, \mu_{\mathrm{DNG}} = -\mu_{\mathrm{DPS}}$), both $k_{x,\mathrm{DNG}}$ and $k_{x,\mathrm{DPS}}$ have equal magnitude. If their branches are chosen such that they have the same sign as well, then from Eq. (2) both r and t become infinite at any point along the integration path (i.e., for any β). This means that the integral in Eq. (5)—and hence the field solution itself—is undefined at any point in space. On the other hand, taking $k_{x,\mathrm{DNG}}$ and $k_{x,\mathrm{DPS}}$ to have opposite signs ($\mathrm{Im}\{k_{x,\mathrm{DNG}}\} > 0$) leads to $r = 0$ and $t = 1$ at any point along the integration path, and to a well-defined field solution—making it the appropriate branch choice. As we later show, this still leads to field contributions that decay at infinity.

We carry the integration for the matched case along the real β axis (from $-\infty$ to ∞). Substituting Eq. (7a) into Eq. (5), and using the well-known identity for the plane wave decomposition of a cylindrical wave ($H_0^{(2)}$ is the zeroth-order Hankel function of the second kind) [30], leads to

$$\psi(x,z) \underset{x<0}{=} \frac{\psi_0}{\pi}\int_{-\infty}^{\infty}\frac{e^{-jk_{x,\mathrm{DPS}}|x+h|}}{k_{x,\mathrm{DPS}}}e^{-j\beta z}d\beta = \psi_0 H_0^{(2)}(k_0\rho_{-h}), \quad (8a)$$

where $k_0 = (\omega/c)\sqrt{\varepsilon_{\mathrm{DPS}}\mu_{\mathrm{DPS}}}$, and $\rho_{-h} = \sqrt{(x+h)^2 + z^2}$; i.e., a cylindrical wave emanates from the source ($x = -h$, $z = 0$) with no reflection from the interface, just as it does in free space.

In between the interface and the image plane ($0 < x < +h$), substituting Eq. (7b) for the integrand and taking $k_{x,\mathrm{DNG}} = -k_{x,\mathrm{DPS}}$ also leads to a cylindrical wave, centered at the image point ($x = +h$, $z = 0$),

$$\psi(x,z) \underset{0<x\le h}{=} \frac{\psi_0}{\pi}\int_{-\infty}^{\infty}\frac{e^{+jk_{x,\mathrm{DPS}}(x-h)}}{k_{x,\mathrm{DPS}}}e^{-j\beta z}d\beta = \psi_0 H_0^{(2)}(k_0\rho_{+h}), \quad (8b)$$

where $\rho_{+h} = \sqrt{(x-h)^2 + z^2}$. This integral converges only for $0 < x \le +h$ ($\mathrm{Im}\{k_{x,\mathrm{DPS}}\} < 0$), implying that Eq. (7b) does not apply past the image plane. At the image point the solution reproduces the logarithmic singularity of the source, indicating that perfect reconstruction indeed takes place there.

To retrieve the solution past the image plane, this resulting singularity must be accounted for, extending Eq. (6b),

$$(\partial_x^2 + k_{x,\mathrm{DNG}}^2)g(x,\beta) = -\mu_0\mu_{\mathrm{DPS}}I_0\delta(x+h), \quad (9)$$

which extends Eq. (7b) accordingly, leading to field contributions that decay past the image,

$$g(x,\beta) \underset{x>0}{=} \frac{2\psi_0}{k_{x,\mathrm{DPS}}}te^{-j(k_{x,\mathrm{DNG}}+k_{x,\mathrm{DPS}})h}e^{-jk_{x,\mathrm{DNG}}(-|x-h|)}, \quad (10)$$

and could be integrated there. This produces the expected analytical continuation of Eq. (8b) to the entire image side ($k_{x,\mathrm{DNG}} = -k_{x,\mathrm{DPS}}$),

$$\psi(x,z) \underset{x>0}{=} \frac{\psi_0}{\pi}\int_{-\infty}^{\infty}\frac{e^{-jk_{x,\mathrm{DPS}}|x-h|}}{k_{x,\mathrm{DPS}}}e^{-j\beta z}d\beta = \psi_0 H_0^{(2)}(k_0\rho_{+h}), \tag{11}$$

a result that could also be directly deduced from matching Eq. (8b) at the image plane (as the medium is homogeneous there).

Equation (11) implies that the transverse electric field is "mirrored" by the interface. However, since the z component of the Poynting vector S_z ($\mathbf{S} = \mathbf{E} \times \mathbf{H}$) flips past the interface due to the permeability sign change (whereas S_x does not), the resulting cylindrical wave around the image is a focusing backwards wave (Fig. 2, red arrows). Its phase fronts propagate outwards from the image point while it carries power inwards. The complementary TM response to a magnetic current line source exhibits the same characteristics.

We therefore obtain that a cylindrical wave emanates from the source outward, penetrating into the DNG side without reflection where it produces a focusing cylindrical wave that perfectly recreates the source singularity at the image point (Fig. 2).

By perfectly reconstructing an image of the source "in reverse," we implicitly require that energy could drain out of the system there (e.g., in practice there would be a detector at the image), for a stationary solution could not exist otherwise. This is a universal characteristic of any perfect lensing. Energy entering a system from a source must dissipate somewhere, and for a perfectly focusing system, by definition, this must occur at the focus. This was discussed in detail by Leonhardt for the Maxwell fish-eye lens [26,27,31]. The necessity of a power drain may look puzzling only because we are more accustomed to either scattering scenarios (waves or beams generated at minus infinity and drained at plus infinity) or conventional constructions—where power is possibly generated at a point source, but never perfectly refocuses, and thus again dissipates at infinity.

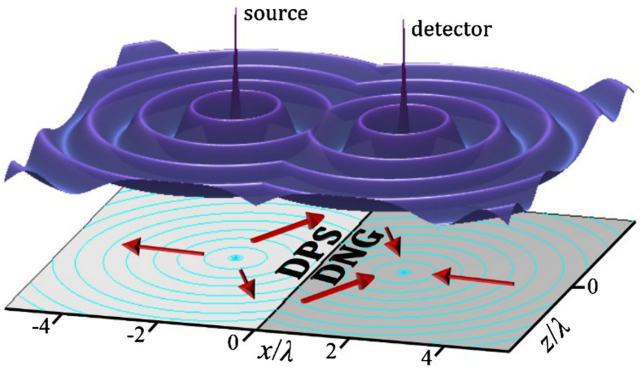

FIG. 2 (color online). The stationary TE field solution for an excitation by a current line source, perfectly "copied" by a matched DPS-DNG single interface onto a drain (average power flow direction shown by red arrows).

We now consider the mismatched scenario. In principle, perfect lensing requires uniform transmission of all spatial frequencies from source to image. As discussed in the previous section, the single-interface configuration maintains an all-pass transmission even with mismatch, though it is only asymptotically uniform. We therefore reexamine the field solution in between the interface and image plane ($0 < x \le h$) and affirm that the source singularity is reproduced at the image despite this nonuniformity.

Substituting Eqs. (7b) and (3) into Eq. (5) (keeping the same branch choice and integration path), we divide the field solution into two contributions, one associated with the asymptotically uniform all-pass transmission and the other with its distortion,

$$\psi(x,z) \underset{0<x\le h}{=} t_\infty \psi_0 H_0^{(2)}(k_0\rho_{+h}) + \frac{\psi_0}{\pi}\int_{-\infty}^{\infty} t_{LP}\frac{e^{+jk_{x,\mathrm{DPS}}(x-h)}}{k_{x,\mathrm{DPS}}}e^{-j\beta z}d\beta, \tag{12}$$

where $t_{LP}(x) = te^{-j(k_{x,\mathrm{DNG}}+k_{x,\mathrm{DPS}})x} - t_\infty$ ($0 < x \le h$) is the nonuniform part of the amplitude transmission from one side of the interface to an equal distance on the other side.

The first term on the rhs of Eq. (12) is a focusing cylindrical wave around the image point [Eq. (8b) multiplied by t_∞], which reproduces the logarithmic source singularity at the image. This singularity is not canceled by the second term, which converges at the image plane ($x = h$) since $t_{LP} \to 0$ for $\beta \to \infty$ ($k_{x,\mathrm{DNG}} \to -k_{x,\mathrm{DPS}}$). Hence, as before, substituting Eq. (10) in Eq. (5) yields the entire image-side field solution,

$$\psi(x,z) \underset{x>0}{=} t_\infty \psi_0 H_0^{(2)}(k_0\rho_{+h}) + \frac{\psi_0}{\pi}\int_{-\infty}^{\infty} t_{LP}\frac{e^{-jk_{x,\mathrm{DPS}}|x-h|}}{k_{x,\mathrm{DPS}}}e^{-j\beta z}d\beta, \tag{13}$$

with $t_{LP}(x) = te^{-j(k_{x,\mathrm{DNG}}+k_{x,\mathrm{DPS}})h}e^{+j(k_{x,\mathrm{DNG}}+k_{x,\mathrm{DPS}})|x-h|} - t_\infty$ ($x > 0$). Despite some field distortion around the image [second term in Eq. (13)] relative to the ideal cylindrical wave form emitted by the source, the source singularity is still completely reproduced at the image point. In other words, the focal spot of a stationary singular source remains singular, even with mismatch.

Since mismatch can be incurred from both material loss and offsets in frequency, this mismatch-immune point-to-point imaging entails both loss immunity and a potentially wide frequency band of operation (depending on the DNG implementation bandwidth). It relies on the single-interface all-pass transmission characteristic. Otherwise, if it had a low-pass transmission (i.e., $t_\infty = 0$), as a mismatched DNG slab does, the image-side singularity would vanish and be replaced by a finite-size focal spot.

Modal interpretation for perfect lensing.—Single-interface perfect lensing can also be understood in terms

of modal analysis. We consider the dispersion relations of both regular modes [32] and Brewster modes [33,34], defined as the poles and zeros of the transverse reflection coefficient, respectively. While regular modes are resonances of the structure (subclassified into confined and leaky), Brewster modes describe scenarios in which the reflected wave contribution vanishes. The regular (+) and Brewster (−) single-interface dispersion relations therefore correspond to the denominator and numerator of r in Eq. (2), respectively (TE) [35],

$$k_{x,\mathrm{DPS}}/\mu_{\mathrm{DPS}} \pm k_{x,\mathrm{DNG}}/\mu_{\mathrm{DNG}} = 0, \tag{14}$$

with the analytical solution [36]

$$\beta = k_0 \sqrt{\frac{\mu_{\mathrm{DNG}}/\mu_{\mathrm{DPS}}}{\mu_{\mathrm{DNG}}/\mu_{\mathrm{DPS}}+1}} \sqrt{\frac{\mu_{\mathrm{DNG}}/\mu_{\mathrm{DPS}} - \varepsilon_{\mathrm{DNG}}/\varepsilon_{\mathrm{DPS}}}{\mu_{\mathrm{DNG}}/\mu_{\mathrm{DPS}}-1}}. \tag{15}$$

The modal field profiles [substituting r into Eq. (1)],

$$f(x) = \begin{cases} e^{\pm jk_{x,\mathrm{DPS}}x} & x < 0 \\ e^{-jk_{x,\mathrm{DNG}}x} & x > 0, \end{cases} \tag{16}$$

fit an outgoing (+) or incoming (−) plane wave in the DPS.

In the matched case ($\varepsilon_{\mathrm{DNG}} = -\varepsilon_{\mathrm{DPS}}$, $\mu_{\mathrm{DNG}} = -\mu_{\mathrm{DPS}}$), the Brewster mode dispersion relation in Eq. (16) is satisfied at any spatial frequency β (i.e., flat dispersion). The smaller the mismatch, the flatter the dispersion curve (Fig. 3), becoming completely flat in the matched case as the simultaneous zero and pole in the rhs of Eq. (15) lead to all values of β on the lhs.

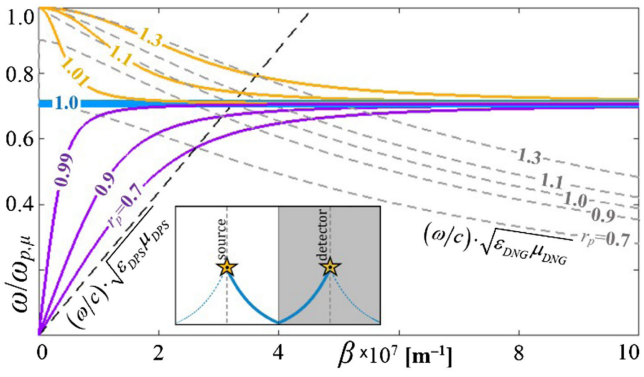

FIG. 3 (color online). TE Brewster mode dispersion curve for a lossless DNG-DPS single interface for different cases (values of $r_p = \omega_{p,\varepsilon}/\omega_{p,\mu}$): $\varepsilon_{\mathrm{DNG}} > \mu_{\mathrm{DNG}}$ (purple lines), $\varepsilon_{\mathrm{DNG}} < \mu_{\mathrm{DNG}}$ (orange lines), and $\varepsilon_{\mathrm{DNG}} = \mu_{\mathrm{DNG}}$ (blue line) exhibiting flat dispersion at the matching frequency. Media light lines: dashed black (DPS) and gray (DNG) lines. Inset: Illustration of single-interface perfect lensing by Brewster mode excitation between the source and image planes. $\varepsilon, \mu_{\mathrm{DNG}} = 1 - \omega_{p,\varepsilon,\mu}^2/\omega^2$, $\varepsilon, \mu_{\mathrm{DPS}} = 1$, $\omega_{p,\mu} = 1.37 \times 10^{16}$ rad/sec.

For a matched single-interface configuration, the Brewster modes are therefore excitable by all incoming plane waves, propagating or evanescent, thereby leading to an all-pass reflectionless transmission. Their field profile decays towards the interface in the DPS ($\mathrm{Im}\{k_{x,\mathrm{DPS}}\} < 0$) and increases in the DNG ($\mathrm{Im}\{k_{x,\mathrm{DPS}}\} > 0$), implying that all incoming plane waves regain their original intensity and phase an equal distance from the interface on the other side—forming there a singular focus. It also agrees with the plane wave decomposition of the Green's function [Eq. (11)] in between the source and image planes (Fig. 3, inset). Single-interface perfect lensing can therefore be attributed to the uniform excitation of single-interface Brewster modes in between the source and image planes.

Conclusions and discussion.—We have presented the case for using a single interface between a passive left-handed material and a conventional dielectric as a perfect lens. Using several complementary analytical methods, we have shown that such a design sustains complete point-to-point mapping from a source onto a detector, despite the inherent material loss or other offsets from the matching condition. Unlike recently published solutions for loss-immune perfect lensing, the single-interface lens does not require the use of gain media or nonlinear effects, and could potentially operate over a wide frequency band.

It may therefore be applied, in principle, to design a superresolution near-field camera. A possible approach could be fabricating a thin left-handed material layer atop a detection layer at the designated image plane. To best approximate the single-interface lens, the detection layer, supplying the necessary power drains, must behave as close as possible to a perfect absorber [37], i.e., to eliminate backscattering such that the left-handed material appears semi-infinite from the source side. Since the intrinsic spatial resolution is infinite, the actual value would be determined by technical parameters—the detection element pixel size, absorption efficiency, exposure time, and the actual left-handed material implementation. Such a design may provide a breakthrough solution for life-science microscopy, lithography, and metrology.

The authors wish to thank B. Simkhovich for useful discussions.

*meiro@ee.technion.ac.il

[1] E. Abbe, Beiträge zur theorie des mikroskops und der mikroskopischen wahrnehmung, Mikrosk. Anat. **9**, 413 (1873).
[2] V. G. Veselago, The electrodynamics of substances with simultaneously negative values of ε and μ, Sov. Phys. Usp. **10**, 509 (1968).
[3] D. R. Smith and N. Kroll, Negative Refractive Index in Left-Handed Materials, Phys. Rev. Lett. **85**, 2933 (2000).
[4] R. A. Shelby, Experimental verification of a negative index of refraction, Science **292**, 77 (2001).

[5] N. Engheta and R. W. Ziolkowski, A positive future for double-negative metamaterials, IEEE Trans. Microwave Theory Tech. **53**, 1535 (2005).
[6] J. B. Pendry, Negative Refraction Makes a Perfect Lens, Phys. Rev. Lett. **85**, 3966 (2000).
[7] D. R. Smith, J. B. Pendry, and M. C. K. Wiltshire, Metamaterials and negative refractive index, Science **305**, 788 (2004).
[8] N. Fang, H. Lee, C. Sun, and X. Zhang, Sub-diffraction-limited optical imaging with a silver superlens, Science **308**, 534 (2005).
[9] T. Taubner, D. Korobkin, Y. Urzhumov, G. Shvets, and R. Hillenbrand, Near-field microscopy through a SiC superlens, Science **313**, 1595 (2006).
[10] R. E. Collin, Frequency dispersion limits resolution in Veselago lens, Prog. Electromagn. Res. B **19**, 233 (2010).
[11] R. Merlin, Analytical solution of the almost-perfect-lens problem, Appl. Phys. Lett. **84**, 1290 (2004).
[12] G. Gómez-Santos, Universal Features of the Time Evolution of Evanescent Modes in a Left-Handed Perfect Lens, Phys. Rev. Lett. **90**, 077401 (2003).
[13] D. R. Smith, D. Schurig, M. Rosenbluth, S. Schultz, S. A. Ramakrishna, and J. B. Pendry, Limitations on subdiffraction imaging with a negative refractive index slab, Appl. Phys. Lett. **82**, 1506 (2003).
[14] R. W. Ziolkowski and E. Heyman, Wave propagation in media having negative permittivity and permeability, Phys. Rev. E **64**, 056625 (2001).
[15] D. J. Bergman, Perfect imaging of a point charge in the quasistatic regime, Phys. Rev. A **89**, 015801 (2014).
[16] V. A. Podolskiy and E. E. Narimanov, Near-sighted superlens, Opt. Lett. **30**, 75 (2005).
[17] P. Tassin, I. Veretennicoff, and G. Van der Sande, Veselago's lens consisting of left-handed materials with arbitrary index of refraction, Opt. Commun. **264**, 130 (2006).
[18] S. Maslovski and S. Tretyakov, Phase conjugation and perfect lensing, J. Appl. Phys. **94**, 4241 (2003).
[19] S. Maslovski and S. Tretyakov, Perfect lensing with phase conjugating surfaces: Towards practical realization, New J. Phys. **14**, 035007 (2012).
[20] J. B. Pendry, Time reversal and negative refraction, Science **322**, 71 (2008).
[21] S. Palomba, S. Zhang, Y. Park, G. Bartal, X. Yin, and X. Zhang, Optical negative refraction by four-wave mixing in thin metallic nanostructures, Nat. Mater. **11**, 34 (2011).
[22] H. Harutyunyan, R. Beams, and L. Novotny, Controllable optical negative refraction and phase conjugation in graphite thin films, Nat. Phys. **9**, 423 (2013).
[23] Y. Urzhumov, C. Ciracì, and D. R. Smith, Nanophotonics: Optical time reversal with graphene, Nat. Phys. **9**, 393 (2013).
[24] H. Alaeian and J. A. Dionne, Parity-time-symmetric plasmonic metamaterials, Phys. Rev. A **89**, 033829 (2014).
[25] R. Fleury, D. L. Sounas, and A. Alù, Negative Refraction and Planar Focusing Based on Parity-Time Symmetric Metasurfaces, Phys. Rev. Lett. **113**, 023903 (2014).
[26] U. Leonhardt, Perfect imaging without negative refraction, New J. Phys. **11**, 093040 (2009).
[27] U. Leonhardt and T. G. Philbin, Perfect imaging with positive refraction in three dimensions, Phys. Rev. A **81**, 011804 (2010).
[28] A. K. Iyer and G. V. Eleftheriades, Free-space imaging beyond the diffraction limit using a Veselago-Pendry transmission-line metamaterial superlens, IEEE Trans. Antennas Propag. **57**, 1720 (2009).
[29] G. Dolling, C. Enkrich, M. Wegener, C. M. Soukoulis, and S. Linden, Low-loss negative-index metamaterial at telecommunication wavelengths, Opt. Lett. **31**, 1800 (2006).
[30] W. C. Chew, *Waves and Fields in Inhomogeneous Media* (Wiley-IEEE Press, New York, 1995).
[31] U. Leonhardt and S. Sahebdivan, Perfect imaging: They do not do it with mirrors, J. Opt. **13**, 024016 (2011).
[32] T. Tamir and A. A. Oliner, Guided complex waves. Part 1: Fields at an interface, Proc. Inst. Electr. Eng. **110**, 310 (1963).
[33] A. Otto, Oberflächenwellen und Brewster fall, Optik (Stuttgart) **38**, 566 (1973).
[34] G. S. Agarwal, New method in the theory of surface polaritons, Phys. Rev. B **8**, 4768 (1973).
[35] R. Ruppin, Surface polaritons of a left-handed medium, Phys. Lett. A **277**, 61 (2000).
[36] I. V. Shadrivov, A. A. Sukhorukov, and Y. S. Kivshar, Nonlinear surface waves in left-handed materials, Phys. Rev. E **69**, 016617 (2004).
[37] Y. Ra'di, C. R. Simovski, and S. A. Tretyakov, Thin Perfect Absorbers for Electromagnetic Waves: Theory, Design, and Realizations, Phys. Rev. Applied **3**, 037001 (2015).